JOURNAL OF SPACECRAFT AND ROCKETS
Vol. 39, No. 2, March–April 2002

Analysis of Bare-Tether Systems for Deorbiting Low-Earth-Orbit Satellites

E. Ahedo* and J. R. Sanmartín†
Universidad Politécnica de Madrid, 28040 Madrid, Spain

Performances, design criteria, and system mass of bare tethers for satellite deorbiting missions are analyzed. Orbital conditions and tether cross section define a tether length, such that 1) shorter tethers are electron collecting practically in their whole extension and 2) longer tethers collect practically the short-circuit current in a fixed segment length. Long tethers have a higher drag efficiency (defined as the drag force vs the tether mass) and are better adapted to adverse plasma densities. Dragging efficiency and mission-related costs are used to define design criteria for tether geometry. A comparative analysis with electric thrusters shows that bare tethers have much lower costs for low- and midinclination orbits and remain an attractive option up to 70 deg.

Nomenclature

A_t = area of tether cross section
$\boldsymbol{B}$ = magnetic field
d_t = width of a thin-tape tether
E_m = motional electric field
$\boldsymbol{F}$ = Lorentz force
F_d = deorbiting force
h_t = thickness of a thin-tape tether
I = current along the tether
i = dimensionless tether current
i_s = inclination of satellite orbit
J_{th} = thermal current density
L_t = tether length
L_{AB} = electron-collecting length of the tether
l_e = electron thermal gyroradius
ℓ_{AB} = dimensionless length of anodic segment
ℓ_t = dimensionless tether length
M = mass
$\dot{m}$ = propellant mass flow rate of an electric thruster
$\dot{m}_C$ = expellant mass flow rate of a cathodic contactor
N_∞ = density of ionospheric plasma
p_t = tether perimeter
R_s = mean radius of satellite orbit
r_b = balloon radius
r_t = radius of a circular-wire tether
T_∞ = temperature of ionospheric plasma
$\boldsymbol{u}_t$ = unit vector along the tether
$\boldsymbol{v}_s$ = satellite velocity
$\boldsymbol{v}_{\text{sp}}$ = specific impulse in velocity units
α = mean tether inclination over local vertical
α_p = relative mass for tankage and plumbing
α_t = relative mass for deployer and ballast
Δh = satellite height drop
δ_d = mass fraction of deorbiting system
η_C = ionization efficiency of cathodic contactor
η_d = drag efficiency
λ_D = debye length
μ_e = power specific mass
Φ = local bias potential between tether and plasma
ϕ = dimensionless bias potential
ρ_t = tether mass density
σ_t = tether conductivity
τ_d = deorbiting time

Subscripts

A = anodic end of the tether
B = zero-potential point in the tether
C = cathodic end of the tether
d = deorbiting system
s = satellite
t = tether
$*$ = reference value

Received 1 February 2001; revision received 25 July 2001; accepted for publication 8 September 2001.

*Associate Professor, Escuela Técnica Superior de Ingenieros Aeronáuticos, Plaza Cardenal Cisneros. Member AIAA.
†Professor, Escuela Técnica Superior de Ingenieros Aeronáuticos, Plaza Cardenal Cisneros.

Introduction

DEORBITING low-Earth-orbiting (LEO) satellites at the end of their operational life as a near-term, feasible and attractive application of electrodynamic tethers was first suggested by Grossi.[1] The bare tether concept appears particularly suitable for that mission due to its simplicity, reliability, and large electron-collection capability.[2,3] The Propulsive Small Expendable Deployer System (ProSEDS) experiment, scheduled for a piggyback flight on a Delta II launch in June 2002, is an attempt to demonstrate the concept suitability by deorbiting the rocket second stage in 2–3 weeks by means of a ~0.4-N electrodynamic drag produced by a 1-2 A current at a 5-km bare aluminum tether.[4] Regarding the principles of operation, the deorbiting mode of a bare tether is just a variation of the generator mode analyzed in the original papers of Sanmartín et al.[2,3] Analyses of subsystems, dynamic control, and reduction in exposed area–time product confirm the feasibility of a bare tether deorbiting system.[5] Vannaroni et al. proposed joint use of a bare tether and a conducting balloon at its anodic end,[6] but recently went back to the simple bare-tether concept, its collection process being both mass efficient and nearly time independent (Kruijff, M., van der Heide, E. J., Vannaroni, G., Dobrowolny, M., and De Venuto, F., private communication, 2001). An early analysis for the generator mode had found only discrete increases in current collection (with an undetermined mass penalty) from adding an electron-collecting device at the end of a bare tether.[7]

This paper presents a general study of the capabilities of bare tethers as deorbiting systems, focusing on 1) tether electrodynamics, 2) design criteria to optimize the drag efficiency, 3) influence of mission requirements and ambient conditions, and 4) operational mass costs of a bare tether compared to electric thrusters. The next section summarizes the principles of operation of a deorbiting tether and discusses the electron-collection capabilities of long tethers and spherical bodies according to up-to-date knowledge. The third section derives the current–voltage (C–V) profiles along the tether, analyzes the regimes of operation, and defines the drag efficiency. The fourth section presents a tradeoff study on dedicated mass of

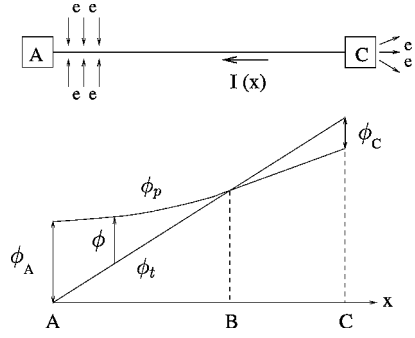

Fig. 1 Scheme of an electrodynamic bare tether operating in the deorbiting or generator modes.

bare tethers and electric thrusters. The last section summarizes the main conclusions.

Principles of Operation

An electrodynamic tether system in orbit around the Earth basically consists of a flexible and conducting tether, tying together two satellites, moving across the geomagnetic field $\boldsymbol{B}$ and exchanging electric current with the surrounding ionosphere. For an orbital velocity $\boldsymbol{v}_s$, the geomagnetic field induces a motional electric field $\boldsymbol{v}_s \wedge \boldsymbol{B}$, in the tether reference frame. This electric field drives an electric current I along the tether, provided that a good, steady electric contact is achieved with the ionospheric plasma (of density N_∞ and single temperature T_∞) (Fig. 1). The current I generates a Lorentz force

$$\boldsymbol{F} = \int_0^{L_t} \boldsymbol{u}_t \wedge \boldsymbol{B} I \, \mathrm{d}s \tag{1}$$

on the tether. Here $\boldsymbol{u}_t(s)$ is the tangent unit vector along the tether, pointing in the direction of the electric current, and L_t is the tether length. The direction of $\boldsymbol{F}$ changes with the direction of the electric current, deorbiting missions requiring $\boldsymbol{F} \cdot \boldsymbol{v}_s < 0$. For an eastward, low-inclination orbit around Earth, this implies the current to flow up the tether. When tether curvature and variations of $\boldsymbol{B}$ along the tether are neglected, the drag force is

$$F_d = -\boldsymbol{F} \cdot \frac{\boldsymbol{v}_s}{v_s} = \frac{E_m}{v_s} \int_0^{L_t} I(s) \, \mathrm{d}s \tag{2}$$

where

$$E_m = \boldsymbol{u}_t \cdot (\boldsymbol{v}_s \wedge \boldsymbol{B}) > 0 \tag{3}$$

is the induced electric field along the tether. For instance, assuming a dipole model for $\boldsymbol{B}$ and a circular orbit of radius R_s and inclination i_s, the average value over many orbits of the induced field is

$$E_m \sim B_E v_{sE} (R_E/R_s)^{\frac{7}{2}} \cos i_s \cos \alpha \tag{4}$$

with α the average inclination of the tether over the local vertical, $B_E \simeq 0.31$ G, $v_{sE} \simeq 7.91$ km/s, and $R_E \simeq 6370$ km magnitudes at the Earth surface.

The typical height range of LEO satellites goes from 750 to 1500 km. For a 1000-km height, E_m is about 150 V/km at $i_s \sim 0$ deg and goes down to 100 V/km at $i_s \sim 45$ deg and to 50 V/km at $i_s \sim 70$ deg. Together with the polar band ($i_s \sim 85$–90 deg), not appropriate for vertical tether systems, the band $i_s \simeq 45$–60 deg presents the largest satellite occupation.[5] Take the 1000-km, midinclination orbit as the typical application case and assume

$$B = 0.3\,\mathrm{G}, \qquad E_m = 100\,\mathrm{V/km}$$
$$N_\infty = 10^{11}\,\mathrm{m}^{-3}, \qquad T_\infty = 0.2\,\mathrm{eV} \tag{5}$$

as nominal ambient conditions to evaluate tether performances throughout the paper. For Eq. (5), the thermal current density (milliampere) is

$$J_{\mathrm{th}} = e N_\infty \sqrt{T_\infty / 2\pi m_e} \simeq 1.2$$

the debye length is $\lambda_D \simeq 1.05$ cm, and the electron thermal gyroradius (centimeter) is

$$l_e = \sqrt{m_e T_\infty}/eB \simeq 3.5$$

If Φ_t is the tether potential, Φ_p the potential of the surrounding plasma in the tether frame, and $\Phi = \Phi_t - \Phi_p$ the potential bias between them, a stationary exchange of electrons with the local ionosphere implies Φ is positive in part of the tether (segment AB in Fig. 1) and is negative in the rest (segment BC). The point where $\Phi = 0$ (point B) is self-adjusted according to plasma conditions. In the simplest bare-tether system, electrons are collected from the ionosphere along anodic segment AB of the tether (of length L_{AB}), and are emitted back at end mass C by some kind of plasma contactor (a hollow-cathode device, for instance).

Electron Collection

The viability and reliability of a tether system relies largely on its capability to collect electrons from the rarefied ionosphere. Hence, it is important to review briefly the state of knowledge and confidence on this issue. To this goal, we consider electron collection by conductive tethers and balloons biased to a potential Φ, positive and large compared to the plasma temperature, $e\Phi/T_\infty \gg 1$.

First, for the case of a long tether the following facts apply:

1) Current collection is bidimensional and proportional to the tether cross-sectional perimeter p_t and anodic length L_{AB}, which makes possible to collect large currents with small cross-sectional sizes.

2) Within a parametric domain (defined later), the current collected by the tether from a Maxwellian plasma follows the orbital-motion-limit (OML) law for cylinders[8]:

$$I = I_{\mathrm{OML}} \simeq J_{\mathrm{th}}\, p_t \int_0^{L_{AB}} G_{\mathrm{OML}} \, \mathrm{d}x, \qquad G_{\mathrm{OML}}(\Phi) \simeq \sqrt{\frac{4e\Phi}{\pi T_\infty} + 1} \tag{6}$$

with G_{OML} the current gain and the x axis along the tether and pointing opposite the electric current (Fig. 1).

3) For a circular tether of radius r_t, the OML law is valid for r_t less than an upper value $r_{t,\max}$, which, for a single temperature plasma and large potential bias, is[9]

$$r_{t,\max} \sim \lambda_D \tag{7}$$

Slightly beyond the OML, the decrease in collected current from the OML value is weak, about a 5% for $r_t = 2r_{t,\max}$.[10] The OML law is applicable to other convex cross sections; for the limit case of a thin tape of width d_t (and thickness h_t, with $h_t \ll d_t$) the OML law is valid for[9]

$$d_t < 4 r_{t,\max} \tag{8}$$

For the same perimeter, a tape has the advantage of a lower mass than the circular wire and the disadvantage of a larger resistance.

4) In a magnetized plasma, the OML law is valid, at least, for[9]

$$\lambda_D \ll l_e, \qquad [\text{and } r_t, d_t/4 \leq \mathcal{O}(\lambda_D)] \tag{9}$$

5) Recent experiments[7,11] confirm that the OML law is satisfied (within a 10% margin) in flowing plasmas as long as the relative velocity is less than the electron thermal speed, which is the case of tethers in LEO orbits, where

$$T_\infty/m_i \ll v_s^2/2 \ll T_\infty/m_e$$

The ion distribution and, therefore, the electric potential structure will be largely anisotropic, but the OML law depends only on the electron distribution, which remains basically Maxwellian.

Next, for the case of a spherical balloon of radius r_b, with $r_b \gg \lambda_D, l_e$, the following facts apply:

1) Current collection is three dimensional, with large currents requiring large balloons, which will make space-charge and magnetic channeling effects dominant.

2) For $r_b \gg \lambda_D$, current collection is far below the OML law for spheres.[8] Instead, for a quiescent, unmagnetized plasma, the Alpert–Lam theory (see Refs. 12 and 13) applies, yielding

$$I = I_{\rm AL} \simeq J_{\rm th}\, 4\pi r_b^2 a G_{\rm AL}^{\frac{6}{7}}, \qquad G_{\rm AL}(\Phi, r_b) = (e\Phi/T_\infty)(\lambda_D/r_b)^{\frac{4}{3}} \tag{10}$$

with factor a about 1.5 for a single-temperature plasma,[14] and with current gain $G_{\rm AL}$ assumed large [$e\Phi/T_\infty \gg (r_b/\lambda_D)^{4/3} \sim 10^3$ for ionospheric tether applications]. Notice that the collected current grows weakly with radius ($I \propto r_b^{6/7}$).

3) LEO ram effects make the electric potential largely anisotropic. This certainly modifies current collection, as evidenced by Tethered Satellite System (TSS)-1 experimental results.[15] However, there is as yet no good theory to quantify ram effects. Because the main effect of plasma motion is the increase of ion energy from $3T_\infty/2$ to $m_i v_s^2/2$ in the quasineutral presheath, a plausible estimate of the current is to apply Eq. (10) with an ion-to-electron temperature ratio of $m_i v_s^2/3T_\infty \sim 15$, which increases factor a in Eq. (10) to 4.6.

4) Because r_b/l_e is very large, magnetic effects need to be considered. Again, there is as yet no consistent theory for current collection by spherical bodies in magnetized, collisionless plasmas at large voltages. The Parker–Murphy theory yields an upper bound for the current[16]:

$$I \le I_{\rm PM}(\Phi) \simeq J_{\rm th} 2\pi r_b^2 G_{\rm PM}$$

$$G_{\rm PM}(\Phi, r_b) \simeq 1 + 2(l_e/r_b)\sqrt{2e\Phi/T_\infty} \tag{11}$$

However, the TSS-1 experiment was a setback for this theory because collected current were 2–3 times larger than the Parker–Murphy bound. Indeed, Vannaroni et al.[15] found TSS-1 results fitting better the Alpert–Lam law for unmagnetized plasmas and, for the balloon configuration, used the empirical law[6]

$$I = I_V \simeq J_{\rm th} 4\pi r_b^2 a_V G_{\rm AL}^{0.472} \tag{12}$$

with $a_V = 4.826$. This expression is uniquely based on TSS-1 results, and there is no clear theory backing it or delimiting its range of validity, in particular with respect to r_b/l_e and λ_D/l_e. The absence of l_e in Eq. (12) makes its application adventurous to configurations different from TSS-1 (300-km height, $r_b = 0.8$ m).

Electron Emission

At present, hollow-cathode devices appear to be the best cathodic contactor technology. In spite of difficulties in reproducing actual space conditions in a laboratory, there is general confidence that emission of large currents at low power cost is not problematic. Proof of this is the selection of a hollow-cathode device capable of emitting a steady current of 10 A to control the floating potential of the International Space Station.[17] The most efficient operational mode of a cathodic contactor is the spot mode, with no current fluctuations, efficient ionization of the emitted expellant, and an almost flat C–V characteristic $\Phi = \Phi_C(I)$. Bias voltages between contactor and plasma lie in the range 15–30 V; in addition, 20–40 W are needed for the keeper circuit.

Electrodynamic Performances

Current and Voltage Profiles

Current and voltage equations are identical for deorbiting and generator modes, but optimum conditions differ widely. Bias potential along the tether, $\Phi = \Phi_t - \Phi_p$, follows

$$\frac{{\rm d}\Phi}{{\rm d}x} = \frac{I}{\sigma_t A_t} - E_m \tag{13}$$

with A_t tether cross-sectional area and σ_t tether conductivity ($\sigma_t \simeq 3.5 \times 10^7\ \Omega^{-1}{\rm m}^{-1}$ for aluminum). If the tether perimeter p_t is small enough, electron collection by the tether follows the OML law (6), with the current profile along segment AB satisfying

$$\frac{{\rm d}I}{{\rm d}x} = eN_\infty \frac{p_t}{\pi}\sqrt{\frac{2e\Phi}{m_e}} \tag{14}$$

The C–V characteristics of the two end masses, $I_A(\Phi_A)$ and $I_C(\Phi_C)$, yield the boundary conditions of the two differential equations.

To solve the tether equations, we introduce three characteristic magnitudes:

$$I_* = E_m \sigma_t A_t, \qquad \Phi_* = E_m L_*$$

$$L_* = \frac{(m_e E_m)^{\frac{1}{3}}}{2^{\frac{7}{3}} e}\left(3\pi \frac{\sigma_t h_t}{N_\infty}\right)^{\frac{2}{3}} \tag{15}$$

where

$$h_t \equiv 2A_t/p_t$$

is thickness for a tape and radius for a circular wire, I_* is the short-circuit current, and Φ_* and L_* are magnitudes gauging ohmic effects for bare tethers [obtained from equating $\frac{3}{4}I_*$ to the OML current, Eq. (6), for a cylinder of (average) bias potential Φ_* and length L_*]. For an aluminum tether, the dimensional values involved in the reference magnitudes can be obtained from

$$I_* \simeq \frac{E_m}{100\ {\rm V/km}} \times \frac{A_t}{1\ {\rm mm}^2} \times 3.5\ {\rm A}$$

$$L_* \simeq \left(\frac{E_m}{100\ {\rm V/km}}\right)^{\frac{1}{3}}\left(\frac{h_t}{0.1\ {\rm mm}}\right)^{\frac{2}{3}}\left(\frac{10^{11}\ {\rm m}^{-3}}{N_\infty}\right)^{\frac{2}{3}} \times 2.66\ {\rm km} \tag{16}$$

Using dimensionless variables

$$i = I/I_*, \qquad \phi = \Phi/\Phi_*, \qquad \xi = x/L_*$$

the tether equations become

$$\frac{{\rm d}\phi}{{\rm d}\xi} = i - 1, \qquad \frac{{\rm d}i}{{\rm d}\xi} = \frac{3}{4}\phi^{\frac{1}{2}} \tag{17}$$

The integration of these equations is straightforward,[3] reducing to a first integral relating i and ϕ and a quadrature for $\xi(\phi)$. Magnitudes of the anodic segment AB satisfy

$$(1 - i_A)^2 - \phi_A^{\frac{3}{2}} = (1 - i_B)^2 \tag{18}$$

$$\frac{L_{AB}}{L_*} \equiv \ell_{AB} = \int_0^{\phi_A} \frac{{\rm d}\phi}{\sqrt{(1 - i_A)^2 - \phi_A^{\frac{3}{2}} + \phi^{\frac{3}{2}}}} \tag{19}$$

For collection at end mass A, we take either $i_A = 0$ or the C–V characteristics of some device, which can be assumed to follow a potential law:

$$i_A(\phi_A) = \beta \phi_A^n \tag{20}$$

with

$$\beta = I_A(\Phi_*)/I_* \tag{21}$$

depending on λ_D/l_e, r_b/l_e (r_b being the device typical size), and n between $\frac{1}{2}$ and $\frac{6}{7}$ for a spherical body.

For ion collection in segment BC, ΔI_{BC}, we have

$$\Delta I_{BC}/I_B \sim \sqrt{(|\Phi_C|/\Phi_A)(m_e/m_i)}$$

Because Φ_C/Φ_A is small for the deorbiting mode (less than 10%, typically), ion collection is doubly negligible, with the electric current remaining constant along segment BC:

$$i \simeq i_C \simeq i_B \tag{22}$$

Integrating Eq. (13) from B to C then yields

$$\phi_C(i_B) = -(1 - i_B)(\ell_t - \ell_{AB}) \tag{23}$$

with

$$\ell_t = L_t/L_* \tag{24}$$

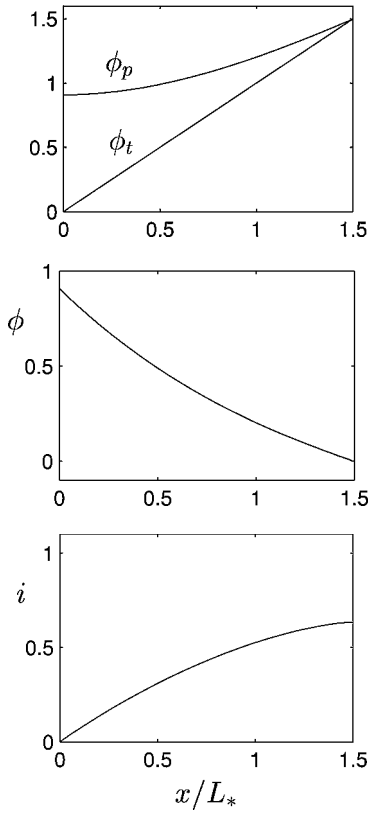

Fig. 2 Voltage and current profiles along the tether for $\ell_t \simeq 1.5$ and $i_A = 0$; maximum current and anode tip voltage: $i_B \simeq 0.63$ and $\phi_A \simeq 0.91$.

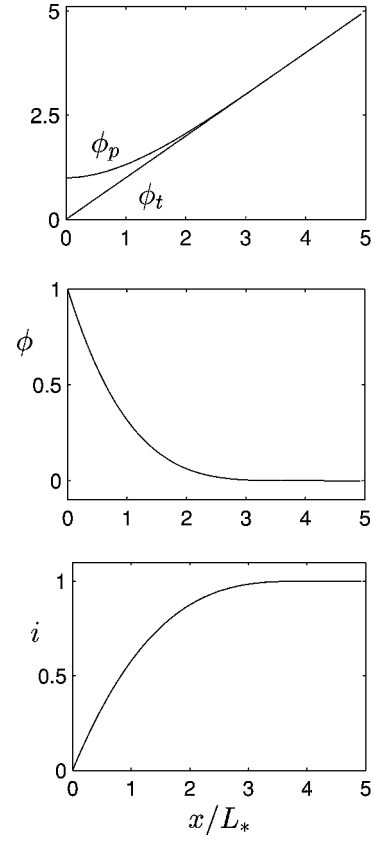

Fig. 3 Voltage and current profiles along the tether for $\ell_t \simeq 5$ and $i_A = 0$; maximum current and tip anode voltage: $i_B \simeq 1$ and $\phi_A \simeq 1$.

the dimensionless tether length and $\phi_C(i)$ the C–V characteristic of end mass C, which involves 1) the contact impedance for the plasma contactor and ionosphere, 2) the wave radiation losses, and 3) the voltage drop at any interposed load. For the deorbiting mode, the only interposed load would be control and power units for the cathodic contactor. For typical design conditions, we have $\phi_C \ll 1$, and the solution for the ideal case $\phi_C = 0$ should approximate actual conditions well.

Equations (18–23) define ϕ_A, i_A, i_B, and ℓ_{AB}, in terms of ℓ_t and end-masses parameters. For the ideal case $\phi_C = 0$, Eq. (23) yields two kinds of distinguished solutions: a short-tether regime (Fig. 2) with

$$\ell_{AB} = \ell_t, \qquad i_B < 1$$

and a long-tether regime (Fig. 3) with

$$i_B = 1, \qquad \ell_{AB} < \ell_t$$

In the short-tether regime, the entire tether is collecting electrons; Φ_t and Φ_p in Fig. 1 meet at an angle at the tether cathodic end. In the long-tether regime, current reaches the short-circuit value ($I_B = I_*$); Φ_t and Φ_p are now tangent at point B and equal beyond. As Figs. 4a and 4b show, Φ_A, L_{AB}, and I_B increase with L_t in the short-tether regime, whereas they become independent of L_t in the long-tether regime.

The transition between both regimes corresponds to the minimum tether length needed to collect the short-circuit current, tip voltage, and anodic length reaching then maximum values, $\phi_{A,\max}$ and $\ell_{AB,\max}$. Figure 5 shows their dependence on parameter β [Eq. (20)] characterizing the C–V characteristic of end mass A. [Equations (16) and (21) indicate that $\beta \sim 0.5$ is already a rather large value for envisaged tether systems.] For a simple bare-tether system with $i_A \simeq 0$, we have $\phi_{A,\max} = 1$ and $\ell_{AB,\max} = 4$, which are absolute maxima. Therefore, Φ_* and $4L_*$ are the maximum anodic tip voltage and length of a tether at given ambient conditions and tether cross section. Figure 5 shows that $\phi_{A,\max}$ decreases significantly with β, thus

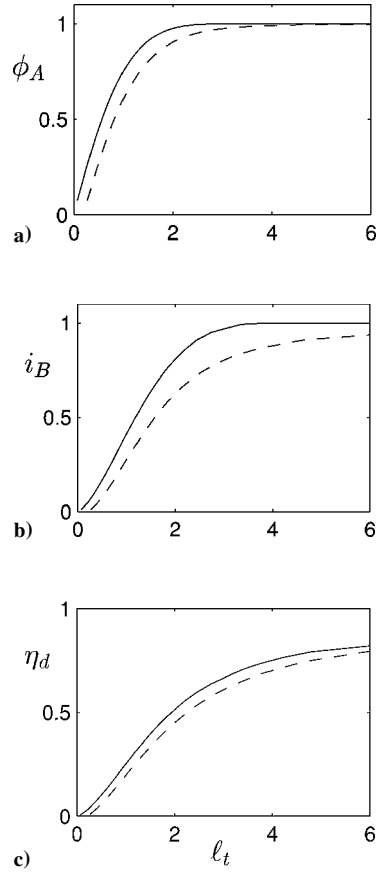

Fig. 4 Influence of tether length on anodic tip voltage, cathode current, and drag efficiency, for $\phi_C = 0$ (——), $\phi_C = -0.2$ (– – –), and $i_A = 0$.

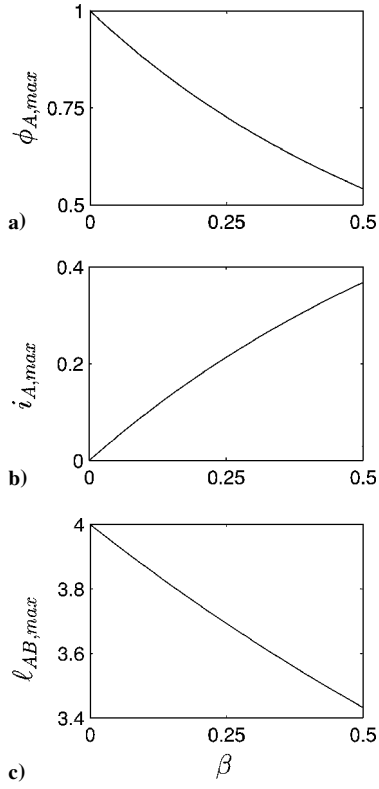

Fig. 5 Influence of the C–V characteristic of end mass A, $i_A = \beta\phi_A^n$, with $n = \frac{1}{2}$, on the maximum values of a) tip voltage, b) end-mass collected current, and c) length of anodic segment.

reducing the collecting capability of both end mass and tether, justifying that $\ell_{AB,\max}$ is affected weakly by β.

Finally, for ϕ_C nonzero but small, the same trends are found, although there is no sudden transition between the two regimes. Figure 4 compares the solutions for $\phi_C \simeq 0$ and $\phi_C(i_B) \simeq \text{const} = -0.2$, confirming that the ideal case provides a good enough approximation.

Drag Efficiency

From Eqs. (2) and (13), the drag exerted on the tether is given by

$$F_d = (I_*/v_s)(E_m L_t - \Phi_A + \Phi_C) \tag{25}$$

A simple figure of merit for different tether designs (with no collection at end mass A) is the ratio of drag F_d on the tether, to tether mass M_t. If ρ_t is tether mass density (about 2800 kg/m^3 for aluminum), one has

$$F_d/M_t \equiv \eta_d g_t, \qquad g_t = (\sigma_t/\rho_t)\left(E_m^2/v_s\right) \tag{26}$$

with

$$\eta_d = 1 - (\phi_A - \phi_C)/\ell_t \tag{27}$$

a convenient measure of drag efficiency.

Coefficient g_t depends on orbital conditions and tether material; for Al and the nominal conditions of Eq. (5), one has $g_t \simeq 0.016$ m/s^2. Of course, the tether is more efficient for low inclination and altitude. Among materials with low production and manufacturing costs, aluminum maximizes the ratio σ_t/ρ_t. Tether geometry affects only the drag efficiency through length parameter ℓ_t [Eq. (24)]. Function $\eta_d(\ell_t)$ is plotted in Fig. 4c. For $\phi_C \ll 1$, the drag efficiency goes from $\eta_d \simeq 3\ell_t^{3/2}$ for $\ell_t \ll 1$ to

$$\eta_d = 1 - 1/\ell_t$$

for $\ell_t \geq 4$, although Fig. 4c shows this long-tether law applying down to $\ell_t \sim 2$. From the behavior of $\eta_d(\ell_t)$, we find that a good design range for the length parameter is $\ell_t \sim 4$–6. Because $\ell_t \propto L_t h_t^{-2/3}$, fixing ℓ_t (for given ambient conditions) relates tether length and thickness, with thinner tethers also shorter. Notice that, for a thin tape, its width d_t is not involved in η_d; we will see later that d_t is determined from the drag force, that is, the electric current, needed for given mission deorbiting specifications.

Plasma density affects the drag efficiency through $\ell_t \propto L_*^{-1} \propto N_\infty^{2/3}$. Variations of one order of magnitude in plasma density are usual in tethers orbiting around Earth. This fact implies that ℓ_t changes by a factor of 4–5 typically, but, if the tether is designed to operate in the long-tether regime for most ambient conditions, the oscillations in η_d (and F_d) are much lower. For instance, when ℓ_t goes from 3 to 15, η_d changes from 0.65 to 0.93 only. These numbers are a clear illustration of the good adaptability of the bare tether to varying plasma conditions: The tether increases both the collecting length and the bias voltage.

Finally, note the different operational and design conditions of the deorbiting and generator modes. In the generator mode, $\phi_C(i_B)$ is large (consisting mainly of the voltage drop at the useful load), losses due to ion collection in the cathodic part amount to about 10%, and the generator efficiency,

$$\eta_{\text{gen}} \simeq i_C|\phi_C|/\ell_t\eta_d$$

(inversely proportional to η_d) indicates that a tradeoff must be made to minimize the drag force and maximize the generated power.[3] Maximum generator efficiency corresponds to $L_{AB}/L_t \sim 1/7$ and $i_B \sim 0.15 - 0.25$, far from the short-circuit value.

Tradeoff Analysis

The bare tether system is compared with electric thrusters as regards dedicated mass M_d with requisites on both allowed deorbiting duration τ_d and total deorbiting impulse $F_d\tau_d$. This impulse is determined by mission parameters M_s (full spacecraft mass) and Δh (deorbiting height drop, down to 250 km). For the present purposes, we just use the relation

$$F_d\tau_d \simeq (v_s/2R_s)M_s\Delta h \tag{28}$$

with v_s/R_s a mean value of the satellite angular velocity. Typical mission values are $M_s\Delta h \sim 10^5$–10^6 kg · km and $F_d\tau_d \sim 0.1$–1 N · week. The tradeoff study here will compare the ratio $M_d/F_d\tau_d$ for different deorbiting systems. Alternatively, mass fractions of deorbiting systems, M_d/M_s, will be compared with the related parameter

$$\delta_d \equiv \frac{M_d}{M_s}\frac{h_*}{\Delta h} = \frac{M_d}{F_d\tau_d}\frac{v_s h_*}{2R_s} \tag{29}$$

with h_* a reference height drop ($h_* = 1000$ km, for instance, yielding $v_s h_*/2R_s \sim 620$ m/s).

Electric Thrusters

Because deorbiting requirements are large, thruster hardware must be considered mission dedicated, not allowing for cost sharing with other operational missions, such as orbit maintenance. The mass of an electric thruster can be written as

$$M_d = (1 + \alpha_p)\dot{m}\tau_d + \mu_e P_e \tag{30}$$

where $\dot{m}$ is the propellant mass flow, α_p is a factor accounting for propellant tankage and plumbing, P_e is the required electric power, and μ_e is the power specific mass, which takes into account the thruster itself, the power processor unit, and any mass penalty on solar arrays and batteries, attributable to the deorbiting mission. Both α_p and μ_e depend on the thruster type, with typical ranges $\alpha_p \sim 0.1$–0.2 and $\mu_e \sim 2$–12 kg/kW (Ref. 18).

The power required for electric propulsion is

$$P_e = v_{\text{sp}}F_d/2\eta \tag{31}$$

where η is thruster efficiency and

$$v_{\text{sp}} \equiv g_E I_{\text{sp}} = F_d/\dot{m} \tag{32}$$

is specific impulse (in velocity units, for convenience), and $g_E = 9.8$ m/s^2.

Table 1 Hall and ion thruster performances for τ_d = six months and $M_s\Delta h = 10^6$ kg · km

Variable	Thruster type	
	Hall	Ion
I_{sp}, s	1600	2700
V_d, V	300	1000
η	0.5	0.65
μ_e, kg/kW	11	13
δ_M, %	5.4	3.8
P_e, kW	0.64	0.83

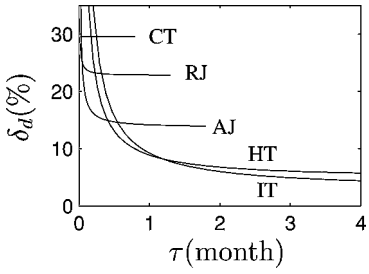

Fig. 6 Estimated mass of different thrusters for deorbiting missions: CT, chemical thruster; RJ, resistojet; AJ, arcjet; HT, Hall thruster; and IT, ion thruster.

Using Eqs. (28–32), we have

$$M_d/F_d\tau_d = (1+\alpha_p)/v_{sp} + (\mu_e/2)(v_{sp}/\eta\tau_d) \qquad (33)$$

which depends only on v_{sp} and τ_d, and is independent of mission requirements, making the comparison between the different thrusters simple and clear. Figure 6 shows δ_d [Eq. (29)] for the most usual types of electric thrusters, in terms of deorbiting time τ_d. Curves are drawn for typical parameters and lifetimes, as taken from Refs. 18 and 19. For chemical propulsion, included for comparison, one would just have the first term on the right-hand side of Eq. (33). Given a deorbiting time, there is a thruster, that is, a specific impulse, that minimizes dedicated mass. As longer deorbiting times are considered, thrusters with larger specific impulses become more attractive. For a given thruster, the first term on the right-hand side of Eq. (33) dominates for τ_d large enough, and there is no significant gain by increasing τ_d further. Because, in general, very short deorbiting times are not an issue, the best options (within the group of electric thrusters) for $\tau_d > 1$ month are Hall or ion thrusters. Table 1 summarizes their typical performances for $\tau_d = 6$ months and $M_s\Delta h \sim 10^6$ kg · km with thrusters operating continuously; ion thrusters present a lower mass but a larger electric power.

Bare Tethers

The mass of a simple bare-tether system, with no collection at the anodic end, is

$$M_d = \dot{m}_C\tau_d(1+\alpha_p) + \alpha_t M_t$$

where we have neglected the contribution of the contactor power unit, $\dot{m}_C$ is the expellant flow rate of the cathodic contactor, and α_t accounts for the mass of the deployer, which can be used at ballast at end of the tether[5]; suggested values for simple deployers are $\alpha_t \sim 2$–2.5. Then, we have

$$M_d/F_d\tau_d = (1+\alpha_p)/v_{sp} + (\alpha_t/g_t)(1/\eta_d\tau_d) \qquad (34)$$

with parameter g_t defined in Eq. (26), and

$$v_{sp} = F_d/\dot{m}_C = \eta_d/i_B \times (I_C/\dot{m}_C)(E_m/v_s) \times L_t \qquad (35)$$

the equivalent specific impulse for the tether system, based in the expellant flow rate. For a long tether, v_{sp} increases linearly with tether length and motional electric field and is favored by a good performance of the cathodic contactor. A tentative law to evaluate the contactor performance is[20]

$$I_C/\dot{m}_C \simeq e\eta_C\Big/\sqrt{m_i m_e} \qquad (36)$$

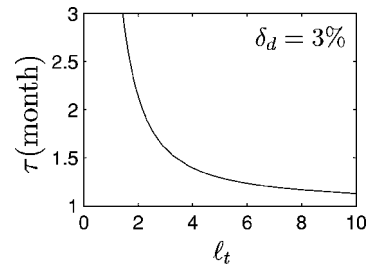

Fig. 7 Bare-tether system: deorbiting time vs dimensionless length for δ_d = 3% and nominal conditions.

with $\eta_C \sim 0.02$–0.05, according to experimental tests on a variety of contactors in the 1–10 A range,[17,21] with the largest efficiencies being for the high-current devices.

For nominal conditions (5) and $\ell_t \sim 3$–10, the tether specific impulse is enormous: $v_{sp} \sim 10^6$ m/s, while one has $g_t/\alpha_t \sim 10^{-2}$ m/s^2. Thus, the last term on the right-hand side of Eq. (34) dominates for deorbiting times up to one year order. Because $g_t \propto E_m^2$, this dominance is stronger for lower values of E_m, which means that, contrary to electric thrusters, the mass related to gas storage is going to be marginal for tethers in their whole range of reasonable deorbiting times. Therefore, to minimize the mass of the bare-tether system, τ_d must be brought to maximum, affordable values and ℓ_t to lie in the long-tether regime.

Because δ_d is mission independent for tethers also, the tradeoff with electric thrusters is simple. According to Fig. 6, a bare-tether system is competitive with electric thrusters for $\delta_d < 3.5\%$. Figure 7 shows τ_d vs ℓ_t for $\delta_d = 3\%$ and nominal conditions (5). Because expellant mass is small, that curve is quasi universal: For other ambient conditions just use

$$\tau_d\delta_d \propto 1\Big/E_m^2\eta_d, \qquad \ell_t^3 \propto E_m h_t^2\Big/N_\infty^2 \qquad (37)$$

The shape of $\tau_d(\ell_t)$ confirms that the tether design parameter ℓ_t must be chosen to be around 3–5 for the worst plasma density conditions.

Figure 8a shows, for $\ell_t = 4$, the dependence of δ_d on deorbiting time and motional electric field; for the approximate relation $i_s(E_m)$, see Eq. (4). For a six-month deorbiting mission, the comparison with electric thrusters shows that the bare tether becomes competitive for $E_m \sim 42$ V/km, that is, $i_s \sim 70$–75 deg, whereas for $E_m > 60$ V/km, that is $i_s < 65$ deg, roughly, the dedicated mass of the bare tether is already below one-half of the ion-thruster mass (or, for the same M_d, we have $\tau_d <$ three months). Although Fig. 8a shows that δ_d can take very low values, these must be taken cautiously because the hardware does not scale down to zero.

Ambient conditions ℓ_t and h_t determine the tether length L_t. Figure 8b shows that, for $h_t = 0.1$ mm, L_t varies in a reasonable interval (7–12 km) for the range of interest of E_m. This result is independent of τ_d; for other values of h_t, just apply $L_t \propto \ell_t h_t^{2/3}$. The variation of the tape width and the collected current are shown in Figs. 8c and 8d for $h_t = 0.1$ mm and $M_s\Delta h = 10^6$ kg · km; for other conditions use the approximate scaling laws

$$d_t \propto \frac{M_s\Delta h}{h_t^{\frac{5}{3}}\tau_d\eta_d E_m^2}, \qquad I_C \propto \frac{M_s\Delta h}{h_t^{\frac{2}{3}}\tau_d\eta_d E_m}$$

Notice that the thinner is the cross section the larger is its width and the current collected. Figures 8c and 8d show that I_C is modest and d_t is well within the validity range of OML law [Eq. (8)]. Therefore, there is a wide margin for a good tether design, which adds reliability to the conclusions extracted from this basic tradeoff analysis.

A measure of tether survivability is the (exposed area)–time product

$$d_t L_t \tau_d \propto 1/h_t\eta_d$$

For a long bare tether, this product is almost unaffected by both deorbiting time and tether length. For the same mass and ambient conditions, thin tapes would have a lower survivability than circular wires, but they are more efficient because of their larger ℓ_t.

Table 2 Performances of four tether designs of similar M_d for nominal conditions

	Case			
Variable	1	2	3	4
r_b, m	2.5	2.5	0	0
L_t, km	5	5	10	20
A_t, mm^2	0.5	0.5	0.5	0.25
h_t, mm	0.4	0.1	0.1	0.1
Φ_A, V	297	189	266	266
I_A, A	0.46	0.37	0	0
I_B, A	0.88	1.5	1.75	0.88
F_d, mN	48.3	73.9	175	206

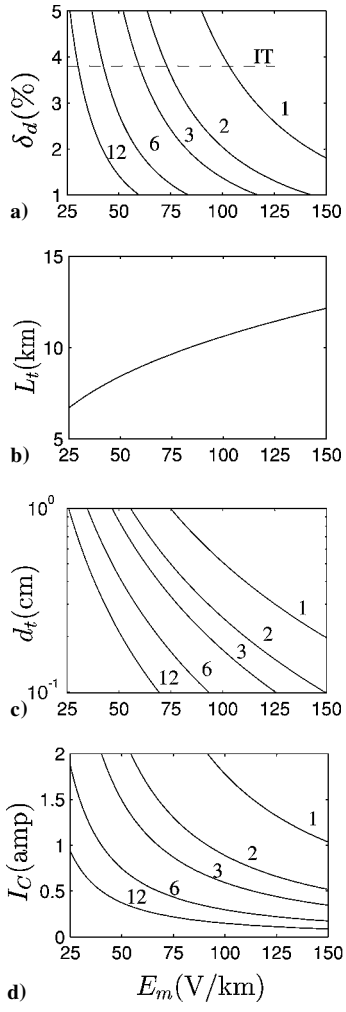

Fig. 8 Bare-tether system: a) dedicated mass fraction; b) tether length, tape thickness $h_t = 0.1$ mm; c) thin-tape width, tape thickness $h_t = 0.1$ mm, $M_s \Delta h/h_* = 1000$ kg; and d) electric current vs motional electric field for $\ell_t = 4$, nominal conditions (5), and $\tau_d = 1, 2, 3, 6$, and 12 months, tape thickness $h_t = 0.1$ mm, $M_s \Delta h/h_* = 1000$ kg.

Bare Tethers with Balloons

Vannaroni et al. had claimed, before some recent work (Kruijff et al., private communication), that a deorbiting system with current collection based mainly in a large deployable balloon significantly enhances the capabilities of electrodynamic tethers.[6] Table 2 compares their balloon plus tether design with other tether designs of the same dedicated mass and shows that a simple tether system is preferable. Design 1 in Table 2 is the one proposed in Ref. 6, with $M_t = 7$ kg and $M_d = 37$ kg, thus allowing 30 kg for tether deployer, balloon, and balloon deployer. Design 2 keeps the balloon and tether masses, but uses a thin tape instead of a circular wire. Designs 3 and 4 eliminate the balloon, duplicate the tether mass (in two different ways), and keep the total mass equal to 37 kg (if 23 kg is allowed just for the tether deployer). Performances in Table 2 are for nominal conditions (5). For the balloon electron collection, we used the uncertain empirical law (12), which possibly overestimates the collected current [because it yields larger currents than the unmagnetized Alpert–Lam law (10)]. Table 2 shows that a good bare-tether design, such as number 4, yields more than four times the drag force of design 1. Even the comparison of designs 2 and 3, with similar tether design and dedicated mass, shows that the simple tether more than doubles the balloon plus tether design. Table 3 shows performances computed for the same four tether designs but a plasma density five times smaller ($N_\infty = 2 \cdot 10^{10}$ m^{-3}). Drag is, of course, smaller for all designs, but the comparison is now more negative for the balloon plus tether, with F_d being nine times smaller for design 1 than for design 4. Notice that, for design 4, F_d decreases just to a 70% when N_∞ decreases to 20%.

Table 3 Performances of four tether designs of similar M_d for $N_\infty = 2 \times 10^{10}$ m^{-3}

	Case			
Variable	1	2	3	4
Φ_A, V	430	384	666	776
I_A, A	0.18	0.17	0	0
I_B, A	0.29	0.32	0.54	0.81
F_d, mN	16.6	27.5	79.4	146

Therefore, balloon plus tether systems 1) are less mass efficient, 2) show a very limited adaptability to plasma density conditions, 3) need two deployment mechanisms, and 4) would require a more reliable knowledge of the balloon collection law.

Conclusions

The C–V response of a bare tether in the deorbiting mode presents two regimes of operations. To have high drag efficiency and good adaptability to variable ambient conditions, tethers must be designed to operate in the long-tether regime ($\ell_t \geq 4$, with ℓ_t being proportional to $N_\infty^{2/3}$). In addition to ℓ_t, tether geometry, that is, L_t, A_t, and h_t, is determined by mission specifications (M_d and $M_s \Delta h$) and type of cross section. Similar efficiencies and dedicated masses are achieved by any cross-sectional form, and so there is no clear choice between thin tape and round wire, for example. Thin tapes lead to smaller tether lengths and anode voltages but higher currents and lower survival probability.

A tradeoff comparison with electric thrusters has shown that bare tethers are by far the cheapest deorbiting option for low- and midinclination orbits ($i_s < 60$ deg), and they remain a competitive option up to $i_s \sim 70$ deg. Additional advantages of the tether are the low gas storage and electric power requirements. The main drawbacks of the tether are deployment and micrometeorite hazards and the dependence on varying ionospheric conditions. However, for typical missions, tether design parameters are well within the range of validity of the OML collection law. This fact, the adaptability of the bare tether, and a tolerance in the deorbiting time, make oscillations of ambient conditions a noncritical issue.

In addition, we have shown that a balloon plus bare-tether system yields lower drag forces, less adaptability, larger mechanical complexity, and larger uncertainties than a simple bare-tether system of the same dedicated mass and adequate design.

Finally, this paper has highlighted the basic aspects of a bare-tether deorbiting system. Detailed studies of optimum tether design, mass estimate, deorbiting time, and system reliability will require careful consideration of issues such as satellite trajectory, solar cycle, dynamic stability, or integration in the satellite.

Acknowledgment

This work was financed by the Dirección General de Enseñanza Superior e Investigación Científica of Spain under Projects PB97-0574-C04-01 and -02.

References

[1]Grossi, M., "Future of Tethers in Space," *Proceedings of 4th International Conference on Tethers in Space*, Science and Technology, Hampton, VA, 1995, pp. 11–23.

[2]Sanmartín, J. R., Ahedo, E., and Martínez-Sánchez, M., "An Anodeless Tether Generator," *Physics of Charged Bodies in Space Plasmas*, Societá Italiana de Física, Bologna, Italy, 1992, pp. 241–248.

[3]Sanmartín, J. R., Martínez-Sánchez, M., and Ahedo, E., "Bare Wire Anodes for Electrodynamic Tethers," *Journal of Propulsion and Power*, Vol. 9, No. 3, 1993, pp. 353–360.

[4]Johnson, L., Estes, R. D., Lorenzini, E., Martínez-Sánchez, M., and Sanmartín, J., "Propulsive Small Expendable Deployer System Experiment," *Journal of Spacecraft and Rockets*, Vol. 37, No. 2, 2000, pp. 173–176.

[5]Forward, R. L., and Hoyt, R. P., "Terminator Tether (TM): A spacecraft Deorbit Device," *Journal of Spacecraft and Rockets*, Vol. 37, No. 2, 2000, pp. 187–196.

[6]Vannaroni, G., Dobrowolny, M., and De Venuto, F., "Deorbiting of LEO Satellites with Electrodynamic Tethers," AIAA Paper 2000-0328, 2000.

[7]Samanta Roy, R. I., Hastings, D. E., and Ahedo, E., "Systems Analysis of Electrodynamic Tethers," *Journal of Spacecraft and Rockets*, Vol. 29, No. 3, 1992, pp. 415–424.

[8]Chung, P. M., Talbot, L., and Touryan, K. J., *Electric Probes in Stationary and Flowing Plasmas*, Springer-Verlag, Berlin, 1975, pp. 10–13.

[9]Sanmartín, J. R., and Estes, R. D., "The Orbital-Motion-Limited Regime of Cylindrical Langmuir Probes," *Physics of Plasmas*, Vol. 6, No. 1, 1999, pp. 395–405.

[10]Estes, R. D., and Sanmartín, J. R., "Cylindrical Langmuir Probes Beyond the Orbital-Motion-Limited Regime," *Physics of Plasmas*, Vol. 7, No. 10, 2000, pp. 4320–4325.

[11]Gilchrist, B. E., Bilen, S. V., and Gallimore, A. D., "Current Collection to Long, Thin Probes in a Dense High-Speed Flowing Plasma," *Space Technology and Applications International Forum-2001*, American Inst. of Physics–Springer-Verlag, New York, 2001, pp. 494–501.

[12]Alpert, Y. L., Gurevich, A. V., and Pitaevski, L. P., "Disturbance of the Plasma and the Electric Field in the Vicinity of a Charged Body at Rest," *Space Physics with Artificial Satellites*, Consultants Bureau, New York, 1965, p. 186.

[13]Lam, S. H., "Unified Theory for the Langmuir Probe in a Collisionless Plasma," *Physics of Fluids*, Vol. 8, No. 1, 1965, pp. 73–87.

[14]Ahedo, E., Sanmartín, J. R., and Martínez-Sánchez, M., "Current Collection by an Active Spherical Electrode in an Unmagnetized Plasma," *Physics of Fluids B*, Vol. 4, No. 12, 1992, pp. 3847–3855.

[15]Vannaroni, G., Dobrowolny, M., Lebreton, J. P., Melchioni, E., de Venuto, F., Harvey, C. C., Iess, L., Guidoni, U., Bonifazi, C., and Mariani, F., "Current–Voltage Characteristics of the TSS-1R Satellite: Comparison with Isotropic and Anisotropic Models," *Geophysical Research Letters*, Vol. 25, No. 5, 1998, pp. 749–752.

[16]Parker, L. W., and Murphy, B. L., "Potential Buildup on an Electron-Emitting Ionospheric Satellite," *Journal Geophysical Research*, Vol. 72, No. 5, 1967, pp. 1631–1636.

[17]Patterson, M. J., Hamley, J. A., Sarver-Verhey, T. R., and Soulas, G. C., "Functional Testing of the Space Station Plasma Contactor," AIAA Paper 94-3308, 1994.

[18]Martínez-Sánchez, M., and Pollard, J. E., "Spacecraft Electric Propulsion: An Overwiew," *Journal of Propulsion and Power*, Vol. 14, No. 5, 1998, pp. 688–699.

[19]Estes, R. D., Lorenzini, E. C., Sanmartín, J., Peláez, J., Martínez-Sánchez, M., Johnson, L., and Vas, I. E., "Bare Tethers for Electrodynamic Spacecraft Propulsion," *Journal of Spacecraft and Rockets*, Vol. 37, No. 2, 2000, pp. 205–215.

[20]Martínez-Sánchez, M., and Hastings, D. E., "A Systems Study of a 100 kW Electrodynamic Tether," *Journal of the Astronautical Sciences*, Vol. 35, No. 1, 1987, pp. 75–96.

[21]Minucci, M., Severi, A., and Capacci, M., "Plasma Contactor Device Family for Space Use Working up to 10A: Review of the Functional Testing Activity," *Proceedings of 4th International Conference on Tethers in Space*, Science and Technology, Hampton, VA, 1995, pp. 873–880.

I. E. Vas
Associate Editor